

1 **Bacterial sensors define intracellular free energies for correct enzyme metalation**

2

3 Deenah Osman^{1,2,†}, Maria Alessandra Martini^{1,†}, Andrew W. Foster^{1,2,†}, Junjun Chen³, Andrew J. P.
4 Scott¹, Richard J. Morton⁴, Jonathan W. Steed², Elena Lurie-Luke¹, Thomas G. Huggins³, Andrew D.
5 Lawrence⁵, Evelyne Deery⁵, Martin J. Warren⁵, Peter T. Chivers^{1,2}, Nigel J. Robinson^{1,2*}

6

7 ¹Department of Biosciences, Durham University, Durham, UK. ²Department of Chemistry, Durham
8 University, Durham, UK. ³Procter and Gamble, Mason Business Center, Cincinnati, Ohio, USA.
9 ⁴Department of Mathematics, Physics and Electrical Engineering, Northumbria University,
10 Newcastle-upon-Tyne, UK. ⁵School of Biosciences, University of Kent, Canterbury, Kent, UK.

11

12 †These authors contributed equally to this work.

13

14 *Correspondence and requests for materials should be addressed to N.J.R. (email:
15 nigel.robinson@durham.ac.uk), or P.T.C. (e-mail: peter.chivers@durham.ac.uk).

16 **There is a challenge for metalloenzymes to acquire their correct metals because some inorganic**
17 **elements form more stable complexes with proteins than do others. These preferences can be**
18 **overcome provided some metals are more available than others. However, while the total**
19 **amount of cellular metal can be readily measured, the available levels of each metal have been**
20 **more difficult to define. Metal-sensing transcriptional regulators are tuned to the intracellular**
21 **availabilities of their cognate ions. Here we have determined the standard free energy for metal**
22 **complex formation to which each sensor, in a set of bacterial metal sensors, is attuned: The less**
23 **competitive the metal, the less favorable the free energy and hence greater availability to which**
24 **the cognate allosteric mechanism is tuned. Comparing these free energies with values derived**
25 **from the metal affinities of a metalloprotein reveals the mechanism of correct metalation**
26 **exemplified here by a cobalt-chelatase for vitamin B₁₂.**

27 Metalloenzymes catalyse approximately half of the reactions of life¹⁻⁴. However, because proteins are
28 flexible they select metals imperfectly and have a common order of affinities with, for example,
29 copper and Zn(II) forming tighter complexes than Mn(II)¹⁻⁴. This raises a question about how cells
30 simultaneously metalate proteins that require tight-binding metals and those that require weaker-
31 binding ones. A solution is for cells to maintain more competitive metals at lower availabilities than
32 less competitive ones². Under these conditions subtle differences in metal affinities between proteins
33 should enable them to acquire different metals, but what are the vital metal availabilities and how can
34 they be measured?

35 Bacterial DNA-binding, metal-sensing transcriptional regulators control the expression of
36 genes encoding proteins of metal homeostasis including transport proteins that import metals which
37 are deficient or export those in excess⁵⁻⁷. Sensitivity is tuned to a buffered, available, intracellular
38 metal concentration, such that when sensitivity is adjusted a sensor ceases to detect any change in
39 metal levels⁸. The metal affinities of sensors (K_1 , Fig. 1a), have previously been used as first
40 approximations of their metal-sensitivities, and such values suggest that Cu(I) and Zn(II) are indeed
41 held to lower availabilities than Mn(II)^{5,6,9}. Furthermore, diverse types of estimate of intracellular
42 metal concentrations from eclectic organisms support a view that the cytosol buffers metals that form
43 more stable complexes to lower concentrations than those that form weaker complexes⁸. For example,
44 fluorescent probes also indicate that cytosolic Cu(I) and Zn(II) are at much lower available
45 concentrations than Mn(II)¹⁰. By further developing an approach that accounts for allostery as well as
46 K_1 , which was used to determine the metal-sensitivities and -specificities of Co(II) and Zn(II) sensors
47 in *Salmonella* Typhimurium (hereafter *Salmonella*)¹¹, the purpose of this work was to measure the
48 sensitivities of a complete set of metal sensors in order to define metal availabilities inside a cell and,
49 by so doing, to understand the mechanism of protein metalation.

50 In the course of this work seven sensors were further characterised in *Salmonella*. For each
51 sensor, the objective was to calculate change in DNA binding (or activation of the two activators) as a
52 function of available intracellular metal concentration. To do this, a complete set of parameters have
53 been measured and combined. At each buffered metal concentration a fraction of each DNA target
54 will be bound to its cognate sensor (θ_D). For the two activators the proportion bound solely to

55 metalated-sensor is the relevant parameter (θ_{DM}), since only the metal bound forms of these activators
56 distort the respective promoters to enable the recruitment of RNA polymerase (Fig. 1b)¹². Since
57 metal- and DNA-binding are allosterically coupled, it should be possible to calculate these fractions
58 (θ_D or θ_{DM}) if the number of sensor molecules per cell (P), the number of promoter targets per cell
59 (D), the affinity of each sensor for its cognate metal (K_1), the affinity for DNA of metal-free and of
60 metal-bound sensor (K_3 and K_4 respectively on Fig. 1a) are all known¹¹. Importantly, metal transfer
61 between the sensors and exchangeable intracellular binding sites (metal buffer), can occur by
62 associative ligand exchange (K_6 to K_9 on Fig. 1a), even when the intracellular milieu buffers a metal
63 to a concentration equating to less than one hydrated ion per cell volume ($<2 \times 10^{-9}$ M for
64 *Salmonella*). Ligand exchange reactions can be rapid, enabling thermodynamic equilibrium to be
65 approached without (slow) metal release to the hydrated state. Here, we have obtained the above
66 thermodynamic values for the set of *Salmonella* metal sensors. All of these parameters were then
67 combined, taking into account any change in sensor abundance with exposure to metal, in order to
68 calculate θ_D or θ_{DM} as a function of metal concentration and hence the tuning of each sensor.

69 The purpose of this work was to understand the mechanism by which proteins acquire the
70 correct metal. The cobalt chelatase for vitamin B₁₂ biosynthesis was used as an exemplar and its
71 affinities for metals determined. In isolation, these affinities suggested that the chelatase should
72 become mis-metalated with copper. But, when values for the chelatase were compared to the buffered
73 intracellular metal availabilities to which the sensors were attuned, the mechanism of correct
74 metalation with cobalt was revealed.

75

76 **RESULTS**

77 **The metals detected by *Salmonella* sensors.**

78 There is experimental evidence that six DNA-binding proteins regulate gene expression in a metal-
79 dependent fashion in *Salmonella*^{11,13,14}. These DNA-binding proteins include two metal-dependent
80 transcriptional activators (the copper efflux regulator CueR and the zinc transcriptional regulator
81 ZntR¹⁵), a metal-dependent de-repressor (the resistance to cobalt and nickel regulator RcnR^{16,17}), and
82 metal-dependent co-repressors (the manganese transport regulator MntR¹⁸, the ferric uptake regulator

83 Fur and the zinc uptake regulator Zur¹⁹⁻²¹). One additional metal-dependent co-repressor (the nickel-
84 responsive regulator NikR) can also be predicted from homology and was therefore included in this
85 study (Supplementary Fig. 1)²². Consensus nucleotide-binding sequences have been identified in the
86 promoters of genes regulated by each sensor (Supplementary Fig. 1b,c). The cognate metals detected
87 by each *Salmonella* sensor were first authenticated by measuring the expression of their target genes
88 by quantitative PCR (qPCR; Fig. 1c) and end-point reverse transcriptase PCR after prolonged (4 to 16
89 h) exposure of cultures to metal concentrations that inhibit growth by $\leq 15\%$ (Supplementary Fig. 2).
90 Transcripts under the control of activators, CueR and ZntR, increased in abundance in response to
91 Cu(I) and Zn(II) respectively, those controlled by de-repressor RcnR, increased in response to Co(II)
92 plus Ni(II), while those controlled by co-repressors MntR, Fur, Zur plus NikR, decreased in
93 abundance in response to Mn(II), Fe(II), Zn(II) and Ni(II) respectively (Fig. 1c and Supplementary
94 Fig. 2d-g).

95

96 **Affinities of sensors that complete a set of values.**

97 Metal and DNA affinities have recently been measured for RcnR and Zur¹¹, and a Cu(I) affinity was
98 previously determined for CueR²³. To enable unknown affinities to be measured, six *Salmonella*
99 sensors were over-expressed and purified to homogeneity (Fig. 1d), including Zur for additional
100 measurements of non-specific DNA binding and the effect of salt on DNA binding affinity. One
101 monomer-equivalent of Ni(II) (Fig. 2a), two monomer-equivalents of Fe(II) (Fig. 2b), and two
102 monomer-equivalents of Mn(II) (Fig. 2c), co-migrated with NikR, Fur and MntR, respectively, during
103 gel-filtration chromatography. Upon titration of NikR (10.6 μM) with Ni(II), a Ni(II)-NikR
104 absorbance feature at 302 nm increased linearly and saturated at $\sim 10 \mu\text{M}$ Ni(II), again indicating a
105 stoichiometry of 1:1 Ni(II):NikR (Fig. 2d,e). Competition between NikR and EGTA for Ni(II)
106 enabled a Ni(II) affinity to be calculated (Fig. 2f, Table 1). Upon titration of Fur (10.3 μM) with
107 Fe(II), fluorescence decreased linearly and saturated at $\sim 20 \mu\text{M}$ Fe(II) consistent with a stoichiometry
108 of 2:1 Fe(II):Fur (Fig. 2g-h). Competition between Fur and nitrilotriacetic acid (NTA) for Fe(II)
109 enabled a Fe(II) affinity to be determined (Fig. 2i, Table 1). The affinity of MntR for Mn(II) was
110 determined by competition with the fluorescent probe mag-fura-2 (Fig. 2j), and a Mn(II)-affinity (6.1

111 $(\pm 0.4) \times 10^{-6}$ M) for mag-fura-2 was separately established by direct titration (Fig. 2k). These data
112 showed that Mn(II) has the weakest affinity for its cognate sensor, relative to other metals and cognate
113 sensors (Table 1).

114 Binding of five sensors to DNA was monitored by fluorescence anisotropy with
115 hexachlorofluorescein-labelled promoter fragments at limiting concentrations (Supplementary Fig. 6).
116 The numbers of multimers (dimer or tetramer) that formed the tightest DNA complexes were also
117 analysed with high ($>0.1 \mu\text{M}$) concentrations of DNA (Supplementary Fig. 7). DNA-binding
118 affinities, K_3 and K_4 , were then determined (Table 1). Metalated co-repressors (NikR, Fur and MntR)
119 (Supplementary Fig. 6f-h), formed tighter DNA complexes than their metal-free forms
120 (Supplementary Fig. 6a-c), confirming their mechanism.

121

122 **Metals change the abundance of two sensors.**

123 Some sensors are auto-regulatory and this variable has not previously been taken into account in
124 determinations of metal sensitivity. The copy number (active multimers) per cell of each of the seven
125 sensors was next determined by quantitative multiple reaction monitoring (MRM) mass spectrometry
126 using cells cultured in the presence and absence of elevated concentrations of cognate metal, P_1 and
127 P_0 respectively (Fig. 3a,b and Supplementary Fig. 8). The data showed that the abundances of the
128 Fe(II) and Co(II) sensors changed significantly in response to metal. In low iron, cells contained
129 approximately ten times more Fur dimers than any other sensor, consistent with its large regulon, and
130 this number more than doubled in elevated iron (Fig. 3b). Similarly, RcnR increased by four-fold in
131 elevated Co(II).

132 We recently developed a method to simultaneously solve the equilibria in Fig. 1a and
133 calculate θ_D or θ_{DM} , as shown in Fig. 1b, at different intracellular buffered Co(II) and Zn(II)
134 concentrations, but this did not account for change in sensor abundance with metal¹¹. For co-repressor
135 Fur this method was used to calculate promoter occupancy (θ_D) at different concentrations of Fe(II) in
136 cells with fixed sensor abundances P_0 , P_1 , and at protein abundance intervals of 10% (Fig. 3c). These
137 data show that occupancy of some Fur-sites require *de novo* synthesis of Fur in elevated iron (~15%:
138 The difference between the maximum values with P_0 and P_1 on Fig. 3c). If the affinity of *Salmonella*

139 Fe(II)-Fur for its DNA sites shows some variation, then the weaker sites will only become occupied as
140 the amount of Fur increases in iron, contributing towards a graded response to iron at different Fur-
141 regulated promoters²⁴. By relating change in sensor abundance to change in promoter occupancy (Fig.
142 3c inset), further equations were derived to incorporate metal-dependent changes in sensor abundance
143 (Supplementary Note 2, Supplementary Dataset). Applying these equations revealed hysteresis
144 modulating sensitivity to Co(II) and Fe(II) (Fig. 3c,d). De-repression by Co(II)-RcnR of its own
145 promoter leads to more RcnR being produced: In turn, increased RcnR suppresses the magnitude of
146 de-repression and so the response calculated with the metal-dependent change of RcnR abundance P_T
147 is attenuated at lower [Co(II)] relative to a model with P_0 alone (Fig. 3d).

148

149 **Low buffered cytosolic metal relative to metal cell⁻¹.**

150 By applying the equations in Supplementary Note 2, via the spreadsheet in Supplementary Dataset,
151 the response of every sensor (θ_D or θ_{DM}) to intracellular buffered concentrations of their cognate metal
152 (K_5) was next calculated from the K_1 , K_2 and K_3 values in Table 1, P_0 and P_1 values in Supplementary
153 Fig. 8b, and number of DNA targets in Supplementary Table 1 (Fig. 4a). The analyses assume that the
154 total amount of buffer and metal are sufficiently high that binding of metal to the sensor has no
155 significant effect on the buffered pool of metal. Simulations using solely metal affinity K_1 matched
156 sensitivity for only two of the sensors and the remainder differed by approximately an order of
157 magnitude, some higher and others lower (Supplementary Fig. 10). Although these differences
158 appeared relatively small on scales spanning eighteen log units, they were sufficient to influence
159 subsequent predictions of metal specificities of the cobalt chelatase CbiK. Protein DNA affinities
160 follow a double log dependence on salt concentration^{25,26}, as shown for Zur and NikR (Supplementary
161 Fig. 11). At 500 mM K^+ plus Na^+ (400 mM plus 100 mM respectively), metal sensitivities of most
162 sensors move closer to predictions obtained using solely K_1 (Supplementary Fig. 12). The
163 experimental conditions used here, 300 mM K^+ plus Na^+ , were chosen to reflect standard internal ion
164 concentrations. Non-halophilic bacteria such as *Salmonella* and *E. coli* maintain a relatively constant
165 intracellular K^+ concentration within the range 200 to 500 mM^{27,28}, with 240 mM K^+ used here, and in

166 standard M9 medium (containing 42 mM Na⁺) internal Na⁺ is in the region of 50 mM²⁷, with 60 mM
167 Na⁺ used here.

168 Does a consideration of sensor-binding to non-specific DNA alter predicted metal
169 sensitivities? The amount of competing non-specific DNA per *E. coli* cell is estimated to be 10⁻⁴ M
170 base pairs, with the remainder occluded for example by other DNA binding proteins²⁹. Non-specific
171 binding to the *nixA* promoter was analysed for Zn(II)-Zur and apo-Zur, then estimated for the other
172 sensors, allowing cubic equations that account for competition from non-specific DNA, to be solved
173 (Supplementary Fig. 13). However, the effect of including non-specific DNA binding on metal-
174 sensitivity was negligible (Supplementary Fig. 13c). MntR was estimated to have the tightest non-
175 specific DNA affinity (due to its relatively tight K_3) which was confirmed experimentally
176 (Supplementary Fig. 13d).

177 Available metal concentrations when each cognate sensor undergoes half of its response (Fig.
178 4a, Supplementary Table 2), are many orders of magnitude lower than total cellular metal expressed
179 as a concentration (Supplementary Table 3), and mostly imply negligible free, fully-hydrated, metals.
180 The apparent total metal concentrations in metal-replete cells are within two orders of magnitude of
181 each other for all metals. In contrast, the buffered available cytosolic metal concentrations to which
182 sensors are attuned vary by fifteen orders of magnitude (Supplementary Table 2 and Fig. 4a): The
183 differences between apparent total metal concentrations and available metal concentrations reflect
184 metal in the buffer, metal that is kinetically trapped and metal that is in non-cytosolic locations.

185 The calculations developed here can be used to better understand graded responses in
186 bacterial metal homeostasis and the relationship between buffered metal concentrations and total
187 metal concentrations. A graded response to decreasing Zn(II) has been described for Zur regulated
188 promoters in *B. subtilis* and *E. coli*^{30,31}. The gradation has been attributed to negative cooperativity
189 between the Zn(II) sites of *B. subtilis* Zur, differing in affinity by ~ 20-fold^{31,32}. Both Zn(II) sites must
190 be occupied for tight binding to the *znuA* promoter but only the first site is needed for the *rpsNB*
191 promoter, which encodes an alternative ribosomal protein that does not require Zn(II) and is part of a
192 Zn(II) sparing mechanism when cytosolic Zn(II) pools are depleted³³. By applying the calculations
193 developed here, the sensitivity of *B. subtilis* Zur on the *znuA* promoter is remarkably similar to

194 *Salmonella* Zur on *znuA*, while regulation of *rpsN* is approximately an order of magnitude more
195 sensitive to intracellular Zn(II) (Supplementary Fig. 14). The greater sensitivity of Zur on the *rpsN*
196 promoter is consistent with a role for the product of *rpsN* in ‘fail-safe’ ribosome synthesis upon
197 Zn(II)-depletion³¹. Similarly, by using the calculations developed here to re-examine regulation by *E.*
198 *coli* Zur, the magnitudes of the differences in Zur responses on *znu* and on a gene encoding a
199 ribosomal protein are estimated to be similar in *E. coli* and in *B. subtilis* (Supplementary Fig. 14). In
200 both bacteria, the Zn(II)-sparing, ribosome-switching mechanisms respond at least an order of
201 magnitude below the buffered Zn(II) concentration that regulates the *znu* promoters, albeit by varying
202 K_1 in *B. subtilis* and K_4 in *E. coli* (Supplementary Fig. 14).

203 In Fig. 4b, a Zn(II) buffer has been simulated by assigning an affinity mid-way between
204 proteins with 50% saturation when the responses of *Salmonella* ZntR and Zur are at 0.5 (Fig. 4a), and
205 the buffer has been assigned a capacity to bind up to a half of the total Zn(II) found in Zn(II)
206 supplemented cells (Supplementary Table 3). The curve thus relates change in available buffered
207 metal concentration to total Zn(II), as the buffer transitions from depleted to saturated. The data points
208 reflect the Zn(II) concentrations at the mid-points of the response curves for *Salmonella* ZntR and Zur
209 (on *znuA*) plus *B. subtilis* Zur on the *rpsNB* promoter. This illustrates that while the magnitude of the
210 differences in buffered Zn(II) concentrations that regulate *Salmonella* ZntR and Zur, plus *B. subtilis*
211 Zur on the *rpsNB* promoter (Fig. 4b), are modest compared to variation between sensors for different
212 metals (Fig. 4a), they become substantial when related to fractional saturation of a cytosolic Zn(II)
213 buffer and hence total Zn(II) cell⁻¹.

214

215 **Metal sensing follows the Irving-Williams series.**

216 The term ‘available intracellular metal concentrations’ has the potential to be misleading because
217 many metals are buffered to less than one hydrated ion per cell (Fig. 4a, Supplementary Table 2).
218 Crucially, the hydrated species is less relevant if metal transfer is associative (Fig. 1a). An alternative
219 is to describe availabilities in terms of standard free energies (ΔG°). By comparing standard free
220 energies, metal partitioning can be explained without reference to metal concentrations. The affinity
221 of an unknown protein (or other molecule: K_A), that would have 50% metal occupancy *in vivo* was

222 therefore calculated from available metal concentrations as derived from the tuning of metal sensors,
223 here at 0.5 of their respective responses (Supplementary Note 3, Supplementary Table 2). The ΔG°
224 associated with metal binding to such a protein is shown, along with values for proteins with 20% and
225 80% occupancy (Fig. 4c). The data presented in Fig. 4c reveal that the metal availabilities to which
226 the set of metal sensors are attuned follows an order which is the inverse of the Irving-Williams series
227 (Supplementary Fig. 15)⁴: The tighter the stability constants in the series, the more favorable the free
228 energies to which the cognate allosteric mechanisms are tuned and hence the lower the metal
229 availabilities. By also converting the metal affinities of proteins or other biomolecules to ΔG° values,
230 a comparison of ΔG° values will predict whether or not any given metal can transfer from the buffer
231 to the molecule, with metals flowing to the molecule with the more favorable ΔG° . A comparison of
232 ΔG° values will similarly identify metals that will be released to the cytosol from antimicrobial
233 ionophores³⁴.

234

235 **Free energies explain metalation of B₁₂ chelatase CbiK.**

236 A third of metalloenzymes acquire metals from delivery proteins and/or contain metal-cofactors that
237 have metal-delivery proteins³⁵. To test whether the values in Fig. 4c can explain how the correct
238 metals partition to a metal-delivery pathway, the metal-affinities, and hence free energies for
239 metalation, ΔG° , were determined for the CbiK cobalt chelatase from *Salmonella*. CbiK inserts cobalt
240 in the anaerobic vitamin B₁₂ biosynthesis pathway^{36,37}. CbiK was over-expressed and purified to
241 homogeneity (Fig. 5a). One monomer-equivalent of Co(II) co-migrated with CbiK during gel-
242 filtration chromatography (Fig. 5b, Supplementary Fig. 16). Competition between CbiK and the
243 fluorescent probe fura-2 for Co(II) enabled a Co(II) affinity to be calculated (Fig. 5c, Supplementary
244 Table 4). Competition between CbiK and mag-fura-2 for Mn(II), Fe(II), Ni(II) and Zn(II) enabled
245 affinities to be determined for Fe(II), Ni(II) and Zn(II), and for Fe(II) this was done in conjunction
246 with an Fe(II)-affinity ($5.3 (\pm 0.65) \times 10^{-6}$ M) for mag-fura-2 that was separately established (Fig. 5d-
247 g, Supplementary Fig. 17, 18 and Supplementary Table 4). CbiK did not show any competition for
248 Mn(II) and an affinity weaker than 20 μ M is established from the co-migration of sub-stoichiometric

249 amounts of Mn(II) with CbiK in gel filtration chromatography when the buffer contained 20 μ M
250 Mn(II), and no associated Mn(II) when the buffer was free of Mn(II) (Supplementary Fig. 16c,d). A
251 mean (\pm s.d.) Cu(I) affinity of $7.7 (\pm 1.3) \times 10^{-14}$ M for CbiK was determined by competition with
252 bicinchoninic acid titrated up to one equivalent of Cu(I), noting that protein precipitation occurred at
253 greater stoichiometries (Fig. 5h). Cu(I) forms substantially the most stable complexes with CbiK in
254 comparison to all other metals including Co(II) (Supplementary Table 4). The affinity for Co(II) is
255 comparable to that for Zn(II) and slightly weaker than Ni(II) (Supplementary Table 4). Viewed in
256 isolation, these values suggest that CbiK will be mis-metalated by ions other than Co(II) and
257 preferentially Cu(I).

258 To understand the mechanism by which CbiK acquires the correct metal, rather than Cu(I)
259 Ni(II) or Zn(II), affinities were converted to ΔG° values and compared to the ΔG° for metalation to
260 which sensors are tuned: For Mn(II) an arrow represents a limiting affinity of 20 μ M or less (Fig. 4c).
261 CbiK only approached the ΔG° for Co(II) estimating 15.4% occupancy (Fig. 4c, Supplementary Table
262 4). All other metals, including Cu(I), showed no significant occupancy with the exception of Fe(II)
263 with an estimated 1% occupancy (Supplementary Table 4). CbiK is known to partly complement
264 bacterial cells missing the CysG iron chelatase for siroheme synthesis³⁸, suggesting that CbiK can,
265 under such circumstances, obtain some Fe(II). The Co(II)-CbiK complex was sufficiently labile that
266 no cobalt remained bound to CbiK post purification, and following re-metalation cobalt was lost in a
267 single purification step (Supplementary Fig. 19), unless the purification buffers were supplemented
268 with 20 μ M cobalt (Fig. 5b). Incubation of CbiK with fura-2 plus Co(II) to give ΔG° for available
269 Co(II) matching the intracellular value shown in Supplementary Table 2, nonetheless gave an
270 occupancy of 15.6 %, close to the anticipated value (Supplementary Fig. 19d). It is formally possible
271 that when vitamin B₁₂ is synthesised anaerobically in *Salmonella* cells, the buffered concentration of
272 Co(II) is elevated with RcnR at greater than 0.5 of its response. When the ΔG° for metalation was
273 approximated solely from the metal affinities of the sensors (K_1), Co(II) ceased to be the preferred
274 metal, switching places with Fe(II) and illustrating the importance of combining all of the parameters
275 (Supplementary Table 4, Supplementary Fig. 20).

276

277 **B₁₂ -metalation requires CbiK when Co(II) is buffered.**

278 The insertion of cobalt into sirohydrochlorin, which occurs in the CbiK-dependent pathway for
279 vitamin B₁₂^{36,37}, can be monitored from changes in intense spectral features and typically from a loss
280 of absorbance at 376 nm (Supplementary Fig. 21a)³⁹. Cobalt sirohydrochlorin formed spontaneously in
281 the presence of Co(II) and this reaction was accelerated by CbiK (Fig. 5i). When Co(II) was buffered
282 to the cellular ΔG° for metalation using nitrilotriacetic acid (Fig. 4c, Supplementary Table 2), the
283 formation of cobalt sirohydrochlorin only occurred in the presence of CbiK (Fig. 5i). The comparison
284 of ΔG° values estimated partial metalation of CbiK with Co(II) under these conditions
285 (Supplementary Table 4). The complete conversion of sirohydrochlorin to its cobalt form reflects
286 subsequent catalysis and kinetic trapping of cobalt. Crucially, when Co(II) was buffered to the cellular
287 ΔG° for metalation in the absence of CbiK, spontaneous formation of cobalt sirohydrochlorin was
288 inhibited revealing the necessity for a chelatase that is correctly poised to acquire Co(II) from the
289 cytosolic buffer (Fig. 5i, Supplementary Fig. 21b). Where the ΔG° gradient between buffer and
290 protein predicts low occupancy, folding and kinetic trapping post-binding can enhance saturation, but
291 loading is predicted to become slower and the risk of mis-metalation may be greater.

292

293 **DISCUSSION**

294 In the course of this work representatives of a set of metal sensors were further characterised in
295 *Salmonella* to enable their metal sensitivities to be determined (Fig. 1c-4a, Supplementary Fig. 6).
296 From these sensitivities the free energies for metalation to which sensors are attuned were derived
297 (Fig. 4c, Supplementary Table 2). Metalation *in vivo* becomes predictable from these values as shown
298 in Fig. 4c. Proteins will acquire the most competitive metal for which ΔG° is favorable relative to the
299 buffer, exemplified here by the cobalt chelatase for vitamin B₁₂, CbiK, which in this manner is
300 predicted to correctly acquire Co(II) rather than tighter binding metals (Fig. 4c, Fig 5, Supplementary
301 Table 4). By this mechanism cells can simultaneously metalate and use enzymes requiring
302 uncompetitive metals at the same time as enzymes that require competitive metals.

303 The fraction of proteins which are under metalated, as predicted for CbiK when RcnR is at
304 0.5 of its response, is currently unknown. If cells commonly synthesise larger amounts of enzymes

305 than become metalated, then these proteins will represent a significant fraction of the buffer.
306 Modulation of enzyme activity through metalation status, as observed in *Streptococcus pneumoniae*
307 where Mn(II)-toxicity is mediated by hypermetalation of protein phosphatase PhpP⁴⁰, also becomes
308 possible for enzymes with ΔG° for metalation close to that of the buffer.

309 The stability order of metal complexes, the Irving-Williams series, is shown for first row
310 essential metals, plus Mg(II), metals commonly required by enzymes (Supplementary Fig. 15)^{3,4}. The
311 notion that the availability of metals in cells will be the inverse of this series is not new^{3,8}, but here
312 this is finally demonstrated from the ΔG° for metalation to which sensors are attuned (Fig. 4c). The
313 series inverts after copper and the *Salmonella* cytosol buffers Zn(II) comparably to Ni(II).

314 A consequence of proteins having tighter affinities for incorrect metals is the risk of mis-
315 metalation. To support the use of metalloenzymes in biotechnology, there is a need to determine the
316 ΔG° for metalation in other cell types making it possible to tune the affinities of proteins, or adjust the
317 metal saturation of the cytosol, for optimal metalation in synthetic biology. Mis-metalation is also a
318 feature of chronic diseases including multiple neurological disorders⁴¹⁻⁴⁴, and there is opportunity to
319 better understand which proteins are susceptible to mal-incorporation of which metals from equivalent
320 ΔG° values for compartments in eukaryotes. In nutritional immunity, excess or deficiencies of metals
321 such as Zn(II) or copper, manganese or iron, limit the growth of pathogens⁴⁵⁻⁴⁹, and there is a history
322 of using metals, chelants and ionophores as antimicrobials⁵⁰. An intriguing concept is that microbes
323 are inherently susceptible to fluctuations in metals due to the need for precise control of relative metal
324 availabilities in order to avoid mis-metalation, over-metalation or under-metalation^{40,45-47}. Knowledge
325 of the ΔG° for metalation inside cells will allow new antimicrobial compounds to be tailored to
326 release or deplete specific metals.

327

328 **Acknowledgements** This work was supported by Biotechnology and Biological Sciences Research
329 Council awards BB/J017787/1, BB/R002118/1 and BB/L009226/1. Interactions with Industrial
330 partners were supported by Biotechnology and Biological Sciences Research Council (BBSRC) award
331 BB/L013711/1 plus a financial contribution from Procter and Gamble (in association with
332 BB/J017787/1 Industrial Partnership Award). Kotryna Svedaite, Department of Biosciences, Durham

333 University, provided technical assistance in the measurements of *in vitro* DNA affinities of ZntR and
334 CueR. Ehmke Pohl and Colin Bain, both of Durham University Department of Chemistry, assisted
335 with structure homology modelling and consideration of standard free energy changes, respectively.
336 *Salmonella enterica* serovar Typhimurium strain SL1344 was provided by Jennifer S. Cavet, School
337 of Biological Sciences, University of Manchester, Manchester, U.K. Elia Fioravanti, Mathematical
338 Institute, University of Oxford, assisted with derivations shown in the Supplementary Note 2. All
339 DNA sequencing was conducted by DBS genomics, Durham University.

340

341 **Author Contributions** D.O. conducted the *in vivo* experiments, bioinformatics analyses and was
342 involved in all *in vitro* measurements of sensor affinities. M.A.M. determined *in vitro* affinities of
343 MntR and Fur. M.A.M., along with D.O., A.W.F. and J.W.S., developed computational methods to
344 determine θ_D and θ_{DM} . R.J.M. along with D.O. generated the MATLAB code relating fractional sensor
345 responses to buffered [metal]. A.J.P.S and P.T.C determined the *in vitro* affinities of NikR. J.C. and
346 T.G.H. performed the MRM tandem mass spectrometry. A.W.F. along with E.D., A.D.L., P.T.C. and
347 M.J.W. performed and co-designed analyses of CbiK. N.J.R. and E.L.-L. conceived the programme.
348 N.J.R., D.O. and A.W.F. drafted the manuscript and, in conjunction with M.A.M., interpreted the
349 significance of the data. N.J.R., with input from P.T.C., had overall responsibility for the design,
350 coordination and management of the project. All authors reviewed the results and edited and approved
351 the final version of the manuscript.

352

353 **Competing Financial Interests Statement.** J.C. and T.G.H. are employees of Procter and Gamble.
354 The collaboration was supported by an Industrial Partnership Award from the BBSRC plus a financial
355 contribution from Procter and Gamble (in association with BBSRC award BB/J017787/1).

356

357 **Main Text References**

358 1 Waldron, K. J., Rutherford, J. C., Ford, D. & Robinson, N. J. Metalloproteins and metal
359 sensing. *Nature* **460**, 823-830 (2009).

- 360 2 Tottey, S. *et al.* Protein-folding location can regulate manganese-binding versus copper- or
361 zinc-binding. *Nature* **455**, 1138-1142 (2008).
- 362 3 Fraústo da Silva, J. J. R. & Williams, R. J. P. *The Biological Chemistry of the Elements: The*
363 *Inorganic Chemistry of Life*. (Oxford University Press, Oxford, 1991).
- 364 4 Irving, H. & Williams, R. J. P. Order of stability of metal complexes. *Nature* **162**, 746-747
365 (1948).
- 366 5 Chandrangsu, P., Rensing, C. & Helmann, J. D. Metal homeostasis and resistance in bacteria.
367 *Nat. Rev. Microbiol.* **15**, 338–350 (2017).
- 368 6 Reyes-Caballero, H., Campanello, G. C. & Giedroc, D. P. Metalloregulatory proteins: metal
369 selectivity and allosteric switching. *Biophys. Chem.* **156**, 103-114 (2011).
- 370 7 Giedroc, D. P. & Arunkumar, A. I. Metal sensor proteins: nature's metalloregulated allosteric
371 switches. *Dalton Trans.*, 3107-3120 (2007).
- 372 8 Foster, A. W. *et al.* A tight tunable range for Ni(II) sensing and buffering in cells. *Nat. Chem.*
373 *Biol.* **13**, 409-414 (2017).
- 374 9 Outten, C. E. & O'Halloran, T. V. Femtomolar sensitivity of metalloregulatory proteins
375 controlling zinc homeostasis. *Science* **292**, 2488-2492 (2001).
- 376 10 Carter, K. P., Young, A. M. & Palmer, A. E. Fluorescent sensors for measuring metal ions in
377 living systems. *Chem. Rev.* **114**, 4564-4601 (2014).
- 378 11 Osman, D. *et al.* Fine control of metal concentrations is necessary for cells to discern zinc
379 from cobalt. *Nat. Commun.* **8**, 1884 (2017).
- 380 12 Ansari, A. Z., Chael, M. L. & O'Halloran, T. V. Allosteric underwinding of DNA is a critical
381 step in positive control of transcription by Hg-MerR. *Nature* **355**, 87-89 (1992).
- 382 13 Ikeda, J. S., Janakiraman, A., Kehres, D. G., Maguire, M. E. & Slauch, J. M. Transcriptional
383 regulation of *sitABCD* of *Salmonella enterica* serovar Typhimurium by MntR and Fur. *J.*
384 *Bacteriol.* **187**, 912-922 (2005).
- 385 14 Osman, D. *et al.* Copper homeostasis in *Salmonella* is atypical and copper-CueP is a major
386 periplasmic metal complex. *J. Biol. Chem.* **285**, 25259-25268 (2010).

- 387 15 O'Halloran, T. & Walsh, C. Metalloregulatory DNA-binding protein encoded by the *merR*
388 gene: isolation and characterization. *Science* **235**, 211-214 (1987).
- 389 16 Iwig, J. S., Rowe, J. L. & Chivers, P. T. Nickel homeostasis in *Escherichia coli* – the *rcnR*-
390 *rcnA* efflux pathway and its linkage to NikR function. *Mol. Microbiol.* **62**, 252-262 (2006).
- 391 17 Iwig, J. S., Leitch, S., Herbst, R. W., Maroney, M. J. & Chivers, P. T. Ni(II) and Co(II)
392 sensing by *Escherichia coli* RcnR. *J. Am. Chem. Soc.* **130**, 7592-7606 (2008).
- 393 18 Que, Q. & Helmann, J. D. Manganese homeostasis in *Bacillus subtilis* is regulated by MntR, a
394 bifunctional regulator related to the diphtheria toxin repressor family of proteins. *Mol.*
395 *Microbiol.* **35**, 1454-1468 (2000).
- 396 19 Althaus, E. W., Outten, C. E., Olson, K. E., Cao, H. & O'Halloran, T. V. The ferric uptake
397 regulation (Fur) repressor is a zinc metalloprotein. *Biochemistry* **38**, 6559-6569 (1999).
- 398 20 Hantke, K. Regulation of ferric iron transport in *Escherichia coli* K12: isolation of a
399 constitutive mutant. *Mol. Gen. Genet.* **182**, 288-292 (1981).
- 400 21 Patzer, S. I. & Hantke, K. The ZnuABC high-affinity zinc uptake system and its regulator Zur
401 in *Escherichia coli*. *Mol. Microbiol.* **28**, 1199-1210 (1998).
- 402 22 Schreiter, E. R. *et al.* Crystal structure of the nickel-responsive transcription factor NikR. *Nat.*
403 *Struct. Biol.* **10**, 794-799 (2003).
- 404 23 Osman, D. *et al.* Generating a metal-responsive transcriptional regulator to test what confers
405 metal sensing in cells. *J. Biol. Chem.* **290**, 19806-19822 (2015).
- 406 24 Pi, H. & Helmann, J. D. Sequential induction of Fur-regulated genes in response to iron
407 limitation in *Bacillus subtilis*. *Proc. Natl. Acad. Sci. U S A* **114**, 12785-12790 (2017).
- 408 25 Record, M. T., Jr., Ha, J. H. & Fisher, M. A. Analysis of equilibrium and kinetic
409 measurements to determine thermodynamic origins of stability and specificity and mechanism
410 of formation of site-specific complexes between proteins and helical DNA. *Methods Enzymol.*
411 **208**, 291-343 (1991).
- 412 26 Campanello, G. C. *et al.* Allosteric inhibition of a zinc-sensing transcriptional repressor:
413 insights into the arsenic repressor (ArsR) family. *J. Mol. Biol.* **425**, 1143-1157 (2013).

414 27 Epstein, W. & Schultz, S. G. Cation Transport in *Escherichia coli*: V. Regulation of cation
415 content. *J. Gen. Physiol.* **49**, 221-234 (1965).

416 28 Su, J., Gong, H., Lai, J., Main, A. & Lu, S. The potassium transporter Trk and external
417 potassium modulate *Salmonella enterica* protein secretion and virulence. *Infect. Immun.* **77**,
418 667-675 (2009).

419 29 Stickle, D. F., Vossen, K. M., Riley, D. A. & Fried, M. G. Free DNA concentration in *E. coli*
420 estimated by an analysis of competition for DNA binding proteins. *J. Theor. Biol.* **168**, 1-12
421 (1994).

422 30 Gilston, B. A. *et al.* Structural and mechanistic basis of zinc regulation across the *E. coli* Zur
423 regulon. *PLoS Biol.* **12**, e1001987 (2014).

424 31 Shin, J.-H. & Helmann, J. D. Molecular logic of the Zur-regulated zinc deprivation response
425 in *Bacillus subtilis*. *Nat. Commun.* **7**, 12612 (2016).

426 32 Ma, Z., Gabriel, S. E. & Helmann, J. D. Sequential binding and sensing of Zn(II) by *Bacillus*
427 *subtilis* Zur. *Nucleic Acids Res.* **39**, 9130-9138 (2011).

428 33 Natori, Y. *et al.* A fail-safe system for the ribosome under zinc-limiting conditions in *Bacillus*
429 *subtilis*. *Mol. Microbiol.* **63**, 294-307 (2007).

430 34 Dalecki, A. G., Crawford, C. L. & Wolschendorf, F. Copper and Antibiotics: Discovery,
431 Modes of Action, and Opportunities for Medicinal Applications. *Adv. Microb. Physiol.* **70**,
432 193-260 (2017).

433 35 Foster, A. W., Osman, D. & Robinson, N. J. Metal preferences and metallation. *J. Biol.*
434 *Chem.* **289**, 28095-28103 (2014).

435 36 Warren, M. J., Raux, E., Schubert, H. L. & Escalante-Semerena, J. C. The biosynthesis of
436 adenosylcobalamin (vitamin B12). *Nat. Prod. Rep.* **19**, 390-412 (2002).

437 37 Frank, S. *et al.* Anaerobic synthesis of vitamin B12: characterization of the early steps in the
438 pathway. *Biochem. Soc. Trans.* **33**, 811-814 (2005).

439 38 Raux, E., Thermes, C., Heathcote, P., Rambach, A. & Warren, M. J. A role for *Salmonella*
440 *typhimurium* *cbiK* in cobalamin (vitamin B12) and siroheme biosynthesis. *J. Bacteriol.* **179**,
441 3202-3212 (1997).

442 39 Lobo, S. A. *et al.* Two distinct roles for two functional cobaltochelatas (CbiK) in
443 *Desulfovibrio vulgaris* hildenborough. *Biochemistry* **47**, 5851-5857 (2008).

444 40 Martin, J. E., Lisher, J. P., Winkler, M. E. & Giedroc, D. P. Perturbation of manganese
445 metabolism disrupts cell division in *Streptococcus pneumoniae*. *Mol. Microbiol.* **104**, 334-348
446 (2017).

447 41 Brown, D. R. *et al.* The cellular prion protein binds copper *in vivo*. *Nature* **390**, 684-687
448 (1997).

449 42 Bush, A. I. The metallobiology of Alzheimer's disease. *Trends Neurosci.* **26**, 207-214 (2003).

450 43 McCarthy, R. C. & Kosman, D. J. Iron transport across the blood–brain barrier: development,
451 neurovascular regulation and cerebral amyloid angiopathy. *Cell Mol. Life Sci.* **72**, 709-727
452 (2015).

453 44 Xiao, T. *et al.* Copper regulates rest-activity cycles through the locus coeruleus-
454 norepinephrine system. *Nat. Chem. Biol.* **14**, 655-663 (2018).

455 45 Hood, M. I. & Skaar, E. P. Nutritional immunity: transition metals at the pathogen–host
456 interface. *Nat. Rev. Microbiol.* **10**, 525-537 (2012).

457 46 Lisher, J. P. & Giedroc, D. P. Manganese acquisition and homeostasis at the host-pathogen
458 interface. *Front. Cell. Infect. Microbiol.* **3**, 91 (2013).

459 47 Wilks, A. & Burkhard, K. A. Heme and virulence: how bacterial pathogens regulate, transport
460 and utilize heme. *Nat. Prod. Rep.* **24**, 511-522 (2007).

461 48 Djoko, K. Y., Ong, C.-l. Y., Walker, M. J. & McEwan, A. G. The role of copper and zinc
462 toxicity in innate immune defense against bacterial pathogens. *J. Biol. Chem.* **290**, 18954-
463 18961 (2015).

464 49 Damo, S. M. *et al.* Molecular basis for manganese sequestration by calprotectin and roles in
465 the innate immune response to invading bacterial pathogens. *Proc. Natl. Acad. Sci. USA* **110**,
466 3841-3846 (2013).

467 50 Lemire, J. A., Harrison, J. J. & Turner, R. J. Antimicrobial activity of metals: mechanisms,
468 molecular targets and applications. *Nat. Rev. Microbiol.* **11**, 371-384 (2013).

469

470 **Figure 1 | Metal binding and DNA binding are coupled to enable *Salmonella* to sense different**
471 **metals. a**, Semi-schematic representation of metal sensors in four allosteric conformations (end states,
472 red) which are thermodynamically coupled: apo (i.e. metal free)-protein (P), metal-protein (PM), apo-
473 protein-DNA (PD) or metal-protein-DNA ((PM)D)⁷. Buffered metals (BM) may exchange to and
474 from proteins via association of the molecules. **b**, The fractions of DNA target sites bound to sensor
475 protein (θ_D) or solely to metalated sensor protein (θ_{DM}). **c**, qPCR (\log_2 fold-change) of *mntS* (regulated
476 by MntR), *iroB* (regulated by Fur), *rcnA* (regulated by RcnR), *nixA* (regulated by NikR), *copA*
477 (regulated by CueR), *znuA* (regulated by Zur) and *zntA* (regulated by ZntR) in cells grown in elevated
478 non-lethal metal concentrations. Data are the mean \pm standard deviation (s.d.) of biologically
479 independent samples (n = 4 for *iroB*, *rcnA*, *copA*, *zntA*; n = 3 for *mntS*, *nixA*, *znuA*; †, not analysed).
480 Symbol shapes represent individual experiments. **d**, Purified sensor proteins analysed by SDS-PAGE
481 (full images in Supplementary Fig. 3b). Using gradient SDS-PAGE n = 1.

482

483 **Figure 2 | Metal affinities that complete a set of values for *Salmonella* metal sensors. a-c**, Gel-
484 filtration (Supplementary Fig. 3c in full) showing co-migration of NikR with Ni(II) (**a**), Fur with
485 Fe(II) and Zn(II) (**b** and Supplementary Fig. 4), MntR with Mn(II) (**c**). n = 1 (**a-c**). **d**, Apo-subtracted
486 spectra of Ni(II)-titrated NikR (10.6 μ M), n = 1 at pH 8.0. **e**, Feature at 302 nm from d, shows linear
487 increase saturating at \sim 10 μ M Ni(II) hence 1:1 Ni(II):NikR stoichiometry. **f**, Representative NikR
488 (13.2 μ M) absorbance (n = 4 independent experiments) in competition for Ni(II) with EGTA (784.3
489 μ M). The fit departs from simulations with K_{Ni} ten-fold tighter or weaker. **g**, Quenching of Fur (10.3
490 μ M) fluorescence emission by Fe(II). n = 3 independent experiments with similar results. **h**, Feature at
491 303 nm from g. **i**, Representative Fur (10.2 μ M) fluorescence in competition for Fe(II) with NTA (100
492 μ M) (n = 4 independent experiments). The fit departs from simulations with K_{Fe} ten-fold tighter or
493 weaker for the first pair (second pair K_{Fe} fixed) and second pair (first pair K_{Fe} fixed) of sites. **j**,
494 Representative mag-fura-2 (1.95 μ M) fluorescence (n = 4 independent experiments) in competition
495 for Mn(II) with MntR (18.7 μ M). The fit departs from simulations with K_{Mn} for MntR ten-fold tighter
496 or weaker. **k**, Mn(II) binding to mag-fura-2 from Supplementary Fig. 5 (n = 4 independent
497 experiments), 1:1, $\lambda_{excitation}$ 380 nm, with simulations ten-fold tighter and ten-fold weaker than the

498 fitted mean (\pm s.d.) K_{Mn} of $6.1 (\pm 0.4) \times 10^{-6}$ M for mag-fura-2. Fitting models in Supplementary Note
499 1.

500

501 **Figure 3 | Metals change the abundance of some sensors to modify regulation. a**, Representative
502 chromatograms following MRM mass-spectrometry of ion transitions for analyte (coloured lines) or
503 isotope-labelled internal standards (grey line, right axis for RcnR) for MntR, Fur, RcnR, NikR, CueR,
504 Zur and ZntR respectively, detected in *Salmonella* cell lysates following prolonged exposure to
505 elevated concentrations of cognate metals ($n = 3$ biologically independent samples, other than CueR
506 where $n = 5$ biologically independent samples, with similar results). Multimeric states are noted in
507 Table 1 footnote. Analyte peptide sequence is shown for each protein. Full chromatograms shown in
508 Supplementary Fig. 9. **b**, Abundance of sensors in control cells in minimal media P_0 (left) and with
509 cognate metal P_1 (right). Values were calculated using calibration curves (Supplementary Fig. 8a)
510 normalised to cell number. Bars and error bars are means and s.d., respectively (shapes represent
511 biologically independent experiments with $n = 3$, except for CueR where $n = 6$ (P_0) and $n = 5$ (P_1)). **c**,
512 Fractional DNA occupancy (θ_D) with Fur as a function of buffered [Fe(II)] using K_1 , K_3 , K_4 , target
513 DNA concentration (Table 1), and either P_0 (light orange line), P_1 (dark orange line) or 10%
514 increments between P_0 and P_1 (grey lines). DNA occupancy (black circles) where [Fur] at any given
515 [cognate metal] (P_T) is linearly proportional to θ_D (inset). θ_{D0} and θ_{D1} (determined using P_0 and P_1),
516 are DNA occupancies at low and high [cognate metal], respectively. For co-repressors (e.g. Fur), θ_{D0}
517 and θ_{D1} are minimum and maximum values (the converse relationship for de-repressors). **d**, A
518 comparison of θ_D with RcnR using P_T (solid blue line) relative to fixed [RcnR] and P_0 (dashed light
519 blue), normalised independently for each curve.

520

521 **Figure 4 | Sensing is tuned to the Irving-Williams series. a**, Calculated responses of CueR, NikR,
522 Zur, ZntR, RcnR, Fur and MntR, as θ_D (or θ_{DM} for ZntR and CueR), to buffered concentrations of
523 Cu(I), Ni(II), Zn(II), Zn(II), Co(II), Fe(II) and Mn(II) respectively within *Salmonella* using metal
524 affinities, DNA affinities, cellular protein and DNA target abundances, in Table 1, Supplementary
525 Fig. 8 and Supplementary Table 1. **b**, Relationship between buffered Zn(II) concentration and total

526 Zn(II) ions in a simulated buffer, showing where *Salmonella* Zur and ZntR, plus *B. subtilis* Zur on the
527 *rpsN* promoter (Supplementary Fig. 14), are calculated to undergo 0.5 of their responses. **c**, Standard
528 free energy change (ΔG°) for formation of a protein-metal (PM) complex, which in the *Salmonella*
529 cytosol, gives 20%, 50% or 80% metalation (θ_P): Zn(II) determined for ZntR (*a*), and Zur (*b*),
530 riboswitch used for Mg(II) (Supplementary Table 2), plus ΔG° for CbiK.

531

532 **Figure 5 | Metalation of CbiK and sirohydrochlorin.** **a**, SDS-PAGE of CbiK (Supplementary Fig.
533 16a). $n = 1$ by gradient SDS-PAGE. **b**, Gel-filtration of CbiK in 20 μM Co(II) (Supplementary Fig.
534 16b) ($n = 3$ independent experiments with similar results). **c**, Fura-2 (12.6 μM) fluorescence ($n = 3$
535 independent experiments) competing for Co(II) with CbiK (8.59 μM). **d**, Mag-fura-2 (11.3 μM)
536 absorbance ($n = 3$ independent experiments) out competing CbiK for Mn(II) (7.38 μM): Fits with and
537 without CbiK overlay. **e**, Mag-fura-2 (6.08 μM) absorbance ($n = 3$ independent experiments)
538 competing for Fe(II) with CbiK (19 μM). **f**, Mag-fura-2 (11.3 μM) absorbance ($n = 3$ independent
539 experiments) competing for Ni(II) with CbiK (7.46 μM). **g**, Mag-fura-2 (11 μM) absorbance ($n = 3$
540 independent experiments) competing for Zn(II) with CbiK (6.84 μM). In **c**, **e-g**, fits depart from K_{metal}
541 ten-fold tighter or weaker noting that Ni(II) approaches the tightest limit for the assay. All models in
542 Supplementary Note 1. **h**, BCA (22.1 μM) absorbance without ($n = 3$ independent experiments) or
543 with ($n = 4$ independent experiments) competition for Cu(I) with CbiK (10 μM). Representative data
544 sets **c-h**. **i**, Conversion of sirohydrochlorin (4.67-5.64 μM) after addition of Co(II) with or without
545 CbiK (5 μM), plus or minus a Co(II)-buffer (data are means of $n = 3$ independent experiments \pm s.d.).
546 Full time course shown in Supplementary Fig. 22.

547

Table 1 | Metal affinities, DNA affinities, allosteric coupling free energies and DNA targets of *Salmonella* metal sensors

Sensor/ Metal	$K_{\text{Metal}} (1/K_1) \text{ (M)}^*$	$K_{\text{DNA}} (1/K_3) \text{ (M)}$ (without metal)	$K_{\text{DNA}} (1/K_4) \text{ (M)}$ (with metal)	ΔG_C (kcal mol ⁻¹)	No. DNA targets [†]
MntR/ Mn(II)	$1.3 (\pm 0.4) \times 10^{-5}$	$8.6 (\pm 1.7) \times 10^{-8}$	$5 \times 10^{-9}\text{§§}$	-1.7 (± 0.1)	4
Fur/ Fe(II)	$5.3 (\pm 0.7) \times 10^{-7}\ddagger$	$2.4 (\pm 0.6) \times 10^{-5}$	$5.6 (\pm 2.1) \times 10^{-8}$	-3.6 (± 0.2)	37
RcnR/ Co(II)	$5.1 (\pm 0.9) \times 10^{-10}\ddagger\ddagger$	$1.5 (\pm 0.8) \times 10^{-7}\ddagger\ddagger$	$1.5 (\pm 0.2) \times 10^{-5}\ddagger\ddagger$	+2.7 (± 0.2) ^{**}	1
NikR/ Ni(II)	$2.5 (\pm 0.4) \times 10^{-12}$	$1.1 (\pm 0.1) \times 10^{-5}$	$9.5 (\pm 0.8) \times 10^{-9}$	-4.2 (± 0.1)	2
CueR/ Cu(I)	$3.3 (\pm 0.7) \times 10^{-19}\ddagger\ddagger$	$3.2 (\pm 1.2) \times 10^{-8}\text{§}$	$3.8 (\pm 1.8) \times 10^{-7}\text{§}$	+1.4 (± 0.4) [§]	3
Zur/ Zn(II)	$6.4 (\pm 0.4) \times 10^{-13}\ddagger\ddagger$	$2.7 (\pm 0.4) \times 10^{-5}\ddagger\ddagger$	$4.1 (\pm 1.0) \times 10^{-8}\ddagger\ddagger$	-3.9 (± 0.2) ^{**}	4
ZntR/ Zn(II)	$3.2 (\pm 0.7) \times 10^{-12}\ddagger\ddagger$	$1.1 (\pm 0.4) \times 10^{-7}$	$7.8 (\pm 1.3) \times 10^{-7}$	+1.2 (± 0.2)	1

548

549 All constants are means \pm s.d., with ‘n’ of independent replicates stated in the legends of Fig. 2 and
 550 Supplementary Fig. 6 (other than values marked ^{**}, see below), and are presented here as dissociation
 551 constants. ΔG_C is the free energy coupling metal binding to DNA binding.

552 *Metal-binding data were fit to models describing a single affinity for the complement of allosterically
 553 effective site(s) of each sensor: This is an apparent average affinity of four sites per MntR dimer, two
 554 per Fur or Zur dimer, two per RcnR tetramer, four per NikR tetramer, and one per CueR or ZntR
 555 dimer. It is noted that two sites appear sufficient for allosteric regulation by MntR on some promoters,
 556 and Supplementary Fig. 14 examines an analogous situation for some Zur-regulated promoters.

557 [†]The identified DNA binding sites for each sensor are listed in Supplementary Information.

558 [‡]For Fur, to fit the data in Fig. 2i, it was necessary to consider sequential Fe(II) binding events to four
 559 sites per Fur dimer, with individual (mean (\pm s.d.)) affinities $1/K_1$ of $2.6 (\pm 0.3) \times 10^{-7}$ M for the two
 560 allosteric sites which was converted to a single value describing the filling of both sites. The
 561 individual (mean (\pm s.d.)) affinities $1/K_1$ of sites three and four was $6.4 (\pm 0.6) \times 10^{-8}$ M.

562 ^{‡‡}Determined previously^{11,23}, limiting values confirmed by low-salt titrations, Supplementary Fig. 11
 563 for Zur.

564 [§]Values are for DNA binding by the first CueR dimer. Mean (\pm s.d.) DNA affinities $1/K_3$ and $1/K_4$ of
 565 the second dimer binding were $1.0 (\pm 0.4) \times 10^{-6}$ M and $3.9 (\pm 1.7) \times 10^{-8}$ M for apo- and Cu(I)-CueR,
 566 respectively.

567 ^{§§}Confirmed by titration with 2 nM DNA (n = 6 independent experiments).

568

569 **Online Methods.**

570 **Determination of transcript abundance.** *Salmonella enterica* serovar Typhimurium strain SL1344
571 (J.S. Cavet, University of Manchester), originally from the *Salmonella* Genetic Stock Centre, was
572 used throughout as wild-type. Media and cultures were prepared in plasticware or acid-washed
573 glassware to minimise trace metal contamination.

574 For *iroB*, *rcnA*, *copA* and *zntA*, overnight cultures in M9 minimal medium, supplemented with
575 thiamine (10 µg ml⁻¹) and L-histidine (20 µg ml⁻¹), were diluted to an OD_{600 nm} of 0.025 in fresh
576 supplemented M9 media and cultured aerobically at 37 °C, with shaking (200 rpm), for 4-5 hours. For
577 *znuA*, 25 µM EDTA was included to chelate basal Zn(II). For *nixA* and *mntS*, 1 × M9 salts, 0.4% w/v
578 glucose, 10 mM sodium fumarate and 10 mM sodium formate was chelex-treated (2-3 hours) before
579 addition of MgSO₄ (2 mM), CaCl₂ (0.1 mM), thiamine (10 µg ml⁻¹) and L-histidinol (1 mM). L-
580 histidinol was an alternative to L-histidine minimising Ni(II)-(L-histidine)₂ entry via NikA⁵¹.
581 Overnight cultures were diluted to an OD_{600 nm} of 0.0001 in fresh media and cultured anaerobically for
582 14 - 16 h at 37 °C in capped microcentrifuge tubes without headspace.

583 Growth media was supplemented with metal salts as appropriate: MnCl₂ (200 µM), FeSO₄ (1
584 µM), CoCl₂ (0.5 µM), NiSO₄ (50 µM), CuSO₄ (25 µM) or ZnSO₄ (50 µM). Metal stocks were
585 quantified by ICP-MS. Under aerobic conditions these concentrations cause minimal growth
586 inhibition^{11,23}, and inhibit growth (final cell density) by ≤15% at the point of RNA extraction
587 (Supplementary Fig. 2a-c). Under anaerobic conditions, 5 µM CoCl₂ and 1 µM CuSO₄ inhibit growth
588 by ≤15% at the point of RNA extraction (Supplementary Fig. 2b). RNA was extracted and cDNA
589 generated using up to 1 µg RNA per reverse-transcriptase reaction (50 µl)¹¹. Controls without reverse
590 transcriptase were generated in parallel. Transcript abundance was assessed by end-point PCR and
591 qPCR using oligonucleotide pairs 1 and 2 (*mntS*), 3 and 4 (*iroB*), 5 and 6 (*rcnA*), 7 and 8 (*nixA*), 9 and
592 10 (*copA*), 11 and 12 (*zntA*), 13 and 14 (*znuA*), and 15 and 16 (*rpoD*) each designed to amplify a 100-
593 200 bp fragment (Supplementary Table 5). End-point PCR fragments were resolved by agarose gel
594 electrophoresis (1.5% w/v agarose) and imaged using a Gel-Doc XR+ gel documentation system.
595 qPCR was conducted with 5 ng cDNA and three technical replicates per reaction¹¹. The fold change,
596 relative to the mean of the control condition for each sensor, was calculated using the 2^{-ΔΔCT} method⁵²,

597 with *rpoD* as a reference. C_T values were calculated with LinRegPCR after correcting for amplicon
598 efficiency⁵³.

599

600 **Protein expression and purification.** Over-expression and purification of RcnR, CueR, ZntR and
601 Zur has been described^{11,23}. The *mntR*, *fur*, *nikR* and *cbiK* coding regions were amplified from
602 *Salmonella* genomic DNA using primers 17-24 (Supplementary Table 5) and ligated into the NdeI
603 (BfaI used to produce NdeI compatible overhang for *cbiK*) and EcoRI sites of pET29a (generating
604 pETmntR, pETfur, pETnikR and pETcbiK, respectively). *E. coli* BL21(DE3) transformed to
605 kanamycin (50 $\mu\text{g ml}^{-1}$) resistance with these plasmids, was cultured (37 °C, 180-200 rpm) in LB.
606 Protein expression was induced with 1 mM IPTG (0.2 mM for pETcbiK), with addition of 50 μM
607 ZnSO_4 (2-3 h).

608 Cells overexpressing Fur were suspended in 300 mM NaCl, 5 mM imidazole, 1 mM Tris(2-
609 carboxyethyl)phosphine hydrochloride (TCEP), 20 mM sodium phosphate buffer pH 7.4, plus
610 protease inhibitor cocktail (Sigma) for lysis. Following lysis and clarification, lysate was applied to 5
611 ml HisTrap FF (GE Healthcare) equilibrated with suspension buffer. Column was washed with
612 suspension buffer (eight column volumes, CV), then suspension buffer containing 10 mM imidazole
613 (2 CV), and 100 mM imidazole (0.9 CV), before elution with suspension buffer containing 300 mM
614 imidazole. Eluate was diluted 1 in 3 with 1 mM TCEP and 10 mM HEPES pH 7.0 before application
615 to a 5 ml Q HP column (GE Healthcare) equilibrated with 100 mM NaCl, 1 mM TCEP, 10 mM
616 HEPES pH 7.0, washed with equilibration buffer (5 CV) and eluted with equilibration buffer
617 containing 1 M NaCl. Fur concentration was estimated via $A_{280\text{ nm}}$ (determined $\epsilon_{280\text{ nm}} = 6,672\text{ M}^{-1}\text{ cm}^{-1}$)
618 before gradual addition of 2 molar equivalents of ZnSO_4 and incubation for 1 h at room temperature
619 (to fill the Zn(II) structural site). EDTA was added to 7.5 mM (to remove excess Zn(II)) and sample
620 incubated overnight at 4 °C. Sample was applied to HiLoad 16/600 Superdex 75 (GE Healthcare)
621 equilibrated in 100 mM NaCl, 0.5 mM TCEP, 10 mM HEPES pH 7.0 (chelex-treated), eluted with the
622 same buffer. Fractions containing dimeric Fur (based on elution volume) were applied to 1 ml Q HP
623 column (GE Healthcare) equilibrated in the same buffer, moved into an anaerobic glovebox, washed

624 with 20 mM NaCl, 80 mM KCl, 10 mM HEPES pH 7.0 (chelex-treated, N₂-purged) (10 CV), before
625 elution with 200 mM NaCl, 800 mM KCl, 10 mM HEPES pH 7.0 (chelex-treated, N₂-purged).

626 Cells overexpressing MntR were suspended in 300 mM NaCl, 10 mM imidazole, 20 mM
627 sodium phosphate buffer pH 7.4, plus 1 mM phenylmethanesulfonyl fluoride (PMSF) for lysis.
628 Following lysis and clarification, lysate was applied to a 5 ml HisTrap HP column (GE Healthcare)
629 equilibrated with suspension buffer. Column was washed with suspension buffer (8 CV) before
630 elution with suspension buffer containing 100 mM imidazole. Sample was applied to HiLoad 16/600
631 Superdex 75 equilibrated with 300 mM NaCl, 10 mM EDTA, 10 mM HEPES pH 7.0 and eluted with
632 the same buffer. Pooled MntR containing fractions were loaded onto 1 ml HiTrap Heparin (GE
633 Healthcare) equilibrated with the size exclusion buffer, washed with gel-filtration buffer (10 CV)
634 before elution with 1 M NaCl, 10 mM EDTA, 10 mM HEPES pH 7.0. Eluate was diluted 1 in 3 with
635 10 mM EDTA, 10 mM HEPES pH 7.0 before application to 1 ml HiTrap Heparin equilibrated with
636 the size exclusion buffer. Column was washed with 60 mM NaCl, 240 mM KCl, 10 mM HEPES pH
637 7.0 (chelex-treated) (10 CV), before elution with 200 mM NaCl, 800 mM KCl, 10 mM HEPES pH
638 7.0 (chelex-treated).

639 Cells overexpressing NikR were suspended in 500 mM NaCl, 10 mM imidazole, 100 mM
640 sodium phosphate buffer pH 8.0. Following lysis and clarification, 100 μM NiCl₂ was added to the
641 lysate which was then applied to 1.5 ml Ni(II)-NTA agarose. Column was washed with suspension
642 buffer (15 CV) and suspension buffer containing 35 mM imidazole (10 CV) before elution with
643 suspension buffer containing 250 mM imidazole, 100 mM NaCl. Eluate was diluted 1 in 2 with 2 mM
644 TCEP, 10 mM HEPES pH 7.5 before application to a 5 ml Q HP column equilibrated with 100 mM
645 NaCl, 2 mM TCEP, 10 mM HEPES pH 7.5, washed with equilibration buffer (5 CV) and eluted with
646 equilibration buffer containing 0.5 M NaCl. EDTA (10 mM) and L-histidine (500 μM) were added (to
647 remove Ni(II)) and sample incubated overnight at 37 °C. Sample was applied to HiLoad 16/600
648 Superdex 75 equilibrated in 100 mM NaCl, 1 mM TCEP, 10 mM HEPES pH 7.5 (chelex-treated) and
649 eluted with the same buffer. Pooled NikR containing fractions were applied to 1 ml Q HP equilibrated
650 in the same buffer and moved into an anaerobic glovebox, washed with 100 mM NaCl, 10 mM

651 HEPES pH 7.5 (chelex-treated, N₂-purged) (10 CV), before elution with 100 mM NaCl, 400 mM
652 KCl, 10 mM HEPES pH 7.5 (chelex-treated, N₂-purged).

653 Cells overexpressing CbiK were suspended in 100 mM NaCl, 1 mM DTT, 5 mM imidazole,
654 20 mM sodium phosphate pH 7.4 plus 1 mM PMSF for lysis. Following lysis and clarification, lysate
655 was applied to HisTrap HP (GE Healthcare) equilibrated with suspension buffer. Column was washed
656 with suspension buffer (10 CV), before elution with suspension buffer containing 300 mM imidazole.
657 EDTA was added to 10 mM and sample incubated at room temperature (2 h). Sample was applied to
658 HiLoad 26/60 Superdex 75 (GE Healthcare) equilibrated in 100 mM NaCl, 1 mM TCEP, 10 mM
659 HEPES pH 7.0 (chelex-treated) and eluted with the same buffer. Peak elution fractions (based on
660 SDS-PAGE analysis) were pooled and applied to 1 ml HiTrap Q HP (GE Healthcare) equilibrated in
661 the same buffer and moved into an anaerobic glovebox. Column was washed with 20 mM NaCl, 80
662 mM KCl, 10 mM HEPES pH 7.0 (chelex-treated, N₂-purged) (20 CV) before elution with 40 mM
663 NaCl, 160 mM KCl, 10 mM HEPES pH 7.0 (chelex-treated, N₂-purged). To produce semi-pure CbiK
664 by anion exchange chromatography cells overexpressing CbiK were suspended in 100 mM NaCl, 1
665 mM TCEP, 10 mM HEPES pH 7.0 plus 1 mM PMSF for lysis. Following lysis and clarification,
666 lysate was applied to 1 ml HiTrap Q HP (GE Healthcare) equilibrated with suspension buffer, column
667 washed with suspension buffer (10 CV), before elution with suspension buffer containing 500 mM
668 NaCl.

669 Protein purity was confirmed by SDS-PAGE. Fur, MntR and CbiK were quantified from A₂₈₀
670 nm and extinction coefficients obtained via quantitative amino acid analysis performed by Alta
671 Bioscience. The extinction coefficient for denatured NikR has previously been determined (*E. coli*
672 NikR, 99% identity)⁵⁴, and was corrected for folded NikR by comparison of A_{280 nm} of folded and
673 denatured NikR. MntR $\epsilon_{280 \text{ nm}} = 7,940 \text{ M}^{-1} \text{ cm}^{-1}$, NikR $\epsilon_{280 \text{ nm}} = 4,398 \text{ M}^{-1} \text{ cm}^{-1}$, CbiK $\epsilon_{280 \text{ nm}} = 24,802$
674 $\text{M}^{-1} \text{ cm}^{-1}$. Thiol and metal content were assayed as previously described¹¹, and all protein samples
675 were $\geq 90\%$ reduced (with the exception of CbiK, MntR has no thiols) and $\geq 95\%$ metal-free (Fur
676 contained ~ 1 molar equivalent of Zn(II)). CbiK was typically $< 90\%$ reduced and none of the
677 cysteines are proximal to the active/metal binding site⁵⁵. All *in vitro* experiments were carried out

678 under anaerobic conditions using chelex-treated and N₂-purged buffers, other than MntR (aerobic,
679 chelex-treated buffers).

680 **Preparation of anaerobic metal stocks.** Concentrations of all metal stocks were determined by ICP-
681 MS. (NH₄)₂Fe(SO₄)₂·6H₂O was dissolved in N₂-purged 0.1% v/v HCl under anaerobic conditions and
682 confirmed to be >90% reduced by titration into an excess (~ 10-fold) of ferrozine, 3 ferrozine: 1 Fe(II)
683 $\epsilon_{562\text{ nm}} = 27,900\text{ M}^{-1}\text{ cm}^{-1}$ ⁵⁶. Dilutions from this stock were prepared daily in N₂-purged ultrapure H₂O
684 and confirmed to be >90% Fe(II). CuCl was prepared as described previously and confirmed to be
685 >95% reduced by titration against bathocuproine sulfonate (BCS)⁵⁷. Other metal salts were dissolved
686 in ultrapure H₂O.

687

688 **Determination of metal stoichiometries and affinities.** All experiments conducted in 100 mM NaCl,
689 400 mM KCl, 10 mM HEPES pH 7.0, with inclusion of 5% v/v glycerol for competition of MntR with
690 mag-fura-2 or at pH 8.0 for NikR gel-filtration chromatography and UV-Vis spectroscopy to
691 determine Ni(II)-binding stoichiometry. Scripts for affinity determinations, for use with Dynafit⁵⁸, are
692 in Supplementary Note 1. Gel-filtration chromatography of NikR, MntR, Fur and CbiK (all 20 μM
693 monomer other than CbiK (10 μM monomer), 0.5 ml, recovery of NikR was routinely <100%) was
694 performed using Sephadex G25 (GE Healthcare), with buffer supplemented with 100 μM MnCl₂
695 (MntR), 50 μM (NH₄)₂Fe(SO₄)₂ (Fur) and either 20 μM CoCl₂, MnCl₂ or un-supplemented (CbiK).
696 Where required, proteins were pre-incubated for 30 min with 20 μM MnCl₂ (CbiK), 1.2 molar
697 equivalents of NiCl₂ (NikR), 100 μM MnCl₂ (MntR) and either 50 μM (NH₄)₂Fe(SO₄)₂ or 1 mM
698 EDTA (Fur). Fractions (0.5 ml) were analysed for metal by ICP-MS and protein by Bradford assay or
699 $A_{280\text{ nm}}$.

700 Increasing concentrations of NiCl₂ were added to solutions of NikR (12.8-15.6 μM) and
701 EGTA, equilibrated overnight at room temperature. Absorbance of Ni(II)-NikR was measured using a
702 λ 35 UV-visible spectrophotometer (PerkinElmer). Data were fit to a model describing NikR
703 competition for one molar equivalent of Ni(II) (per monomer) using Dynafit⁵⁸. EGTA Ni(II)-affinity =
704 $4.98 \times 10^{-10}\text{ M}$ at pH 7.0 determined using Schwarzenbach's α co-efficient.

705 (NH₄)₂Fe(SO₄)₂ was titrated into Fur solution in the absence (10-18 μM Fur; to determine
706 Fe(II) stoichiometry), or presence (10-11 μM Fur) of nitrilotriacetic acid (NTA). Fur fluorescence
707 emission was recorded at equilibrium (Cary Eclipse fluorescence spectrophotometer (Agilent
708 Technologies), λ_{ex} = 276 nm, 25 °C). Data were fit to a model describing Fur competition for two
709 molar equivalent of Fe(II) using Dynafit⁵⁸, with positive cooperativity between two pairs of sites per
710 dimer. NTA Fe(II)-affinity = 6.77 × 10⁻⁷ M at pH 7.0 determined using Schwarzenbach's α co-
711 efficient.

712 MnCl₂ was titrated into a solution of mag-fura-2 in the absence (to determine mag-fura-2
713 Mn(II)-affinity) or presence of MntR (7.1-18.7 μM). Mag-fura-2 (ε_{369 nm} = 22,000 M⁻¹ cm⁻¹²³)
714 fluorescence excitation was recorded at equilibrium (Cary Eclipse fluorescence spectrophotometer,
715 λ_{em} = 505 nm, 20 °C). Data were fit to a model describing 1:1 Mn(II):mag-fura-2 stoichiometry and
716 MntR competition for two molar equivalents of Mn(II) per monomer, using Dynafit⁵⁸; mag-fura-2 K_{Mn}
717 = 6.1 (±0.4) × 10⁻⁶ M.

718 MnCl₂, (NH₄)₂Fe(SO₄)₂, NiCl₂ or ZnSO₄ were titrated into a solution of mag-fura-2 in the
719 presence of CbiK and absorbance (325 and 366 nm) recorded at equilibrium (λ₃₅ UV-visible
720 spectrophotometer). Data were fit to models describing 1:1 metal:mag-fura-2 and 1:1 metal:CbiK
721 stoichiometry, using Dynafit⁵⁸; mag-fura-2 K_{Ni} = 5 × 10⁻⁸ M⁵⁹, K_{Zn} = 2 × 10⁻⁸ M²³, and K_{Fe} = 5.3 × 10⁻⁶
722 M (determined by direct titration of mag-fura-2 with (NH₄)₂Fe(SO₄)₂).

723 CoCl₂ was titrated into a solution of fura-2 (ε_{363 nm} = 28,000 M⁻¹ cm⁻¹²³) in the presence of
724 CbiK and fluorescence emission recorded at equilibrium (Cary Eclipse fluorescence
725 spectrophotometer, λ_{ex} = 360 nm, 20 °C). Data were fit to a model describing 1:1 Co(II): fura-2 and
726 1:1 Co(II):CbiK stoichiometry, using Dynafit⁵⁸; fura-2 K_{Co} = 8.6 × 10⁻⁹ M²³.

727 CuCl was titrated into a solution of bicinchoninic acid (BCA) and absorbance of Cu(I):BCA₂
728 (ε_{562 nm} = 7,900 M⁻¹ cm⁻¹⁶⁰) recorded at equilibrium (λ₃₅ UV-visible spectrophotometer). Precipitation
729 at [CuCl] greater than 1:1 Cu(I):CbiK precluded data fitting so CbiK K_{Cu} was determined from
730 individual equilibrium values using Equation 1:

731
$$K_D\beta_2 = \frac{\left(\frac{[P]_{total}}{[MP]}\right) - 1}{\left\{\left(\frac{[L]_{total}}{[ML_2]}\right) - 2\right\}^2 [ML_2]} \quad (1)$$

732 Where $[P]_{total}$ and $[L]_{total}$ are the total concentrations of CbiK and BCA, respectively, K_D is the Cu(I)
 733 dissociation constant of CbiK, β_2 is the formation constant of Cu(I):BCA₂ ($10^{17.2} \text{ M}^{-2}$ ⁶⁰), and $[MP]$
 734 and $[ML_2]$ are the equilibrium concentrations of Cu(I):CbiK and Cu(I):BCA₂ determined $\epsilon_{562 \text{ nm}}$ and
 735 mass balance.

736

737 **Determination of DNA-binding affinities by fluorescence anisotropy.** Fluorescently labelled
 738 double-stranded DNA probes were generated using oligonucleotides 25 and 26 (*nixA*Pro for NikR and
 739 as a non-specific probe for Zur), 27 and 28 (*mntS*Pro for MntR), 29 and 30 (*copA*Pro for CueR), 31
 740 and 32 (*zntA_long*Pro, containing an extended sequence compared to that used previously¹¹, for
 741 ZntR), 33 and 34 (*furbox*, containing the consensus *E. coli* Fur binding site for Fur), 39 and 40
 742 (*mntS*Proswap, a semi-randomised variant of *mntS*Pro for MntR), and 41 and 42 (*znuA*Pro for Zur)
 743 (Supplementary Table 5). In each case one oligonucleotide was hexachlorofluorescein labelled.
 744 Complementary single-stranded oligonucleotides were annealed as described previously¹¹. All
 745 experiments, other than with Zur and some with NikR (as noted in figure legend), were conducted in
 746 60 mM NaCl, 240 mM KCl, 10 mM HEPES pH 7.0, with inclusion of 200 μM MnCl₂ for Mn(II)-
 747 MntR, 5-50 μM (NH₄)₂Fe(SO₄)₂ for Fe(II)-Fur, 1 mM EDTA for apo-NikR, or 5 mM EDTA for all
 748 other apo-proteins. NikR was prepared in 100 mM NaCl, 400 mM KCl, 10 mM HEPES pH 8.0 with
 749 0.95 molar equivalents of NiCl₂ for Ni(II)-NikR. Zur was prepared as described previously¹¹. All other
 750 proteins were prepared in 200 mM NaCl, 800 mM KCl, 10 mM HEPES pH 7.0, with 1.2 molar
 751 equivalents of CuCl for Cu(I)-CueR, 1.2 molar equivalents of ZnSO₄ for Zn(II)-ZntR, 2.2 molar
 752 equivalents MnCl₂ for Mn(II)-MntR, 2.2 molar equivalents of (NH₄)₂Fe(SO₄)₂ for Fe(II)-Fur, and 5
 753 mM EDTA for apo-MntR and apo-Fur. Proteins were titrated against labelled DNA probes and
 754 anisotropy measured using a modified Cary Eclipse Fluorescence Spectrophotometer (Agilent
 755 Technologies), settings described previously²³. For Fur, NikR, CueR, Zur and ZntR, DNA-binding
 756 affinities were determined using Dynafit⁵⁸ (Supplementary Note 1). For MntR, data were fit to a 2nd

757 degree polynomial regression and limits for DNA affinities determined at the intersection of the
758 regression line and half the Δr_{obs} value associated with binding of a MntR dimer to *mntS*Pro. Coupling
759 free energies (ΔG_{C}) were derived as previously described²³.
760
761 **Determination of sensor protein abundance.** Generation of *E. coli* strains BW25113 $\Delta zntR/\Delta zur$
762 (lacking *zntR* and *zur*), BW25113 $\Delta nikR/\Delta rcnR$ (lacking *nikR* and *rcnR*), and *Salmonella* strain
763 SL1344 $\Delta cueR/\Delta golS$ (lacking *cueR*) have been described previously^{11,14}. *E. coli* strains
764 BW25113 $\Delta fur::kan$ (lacking *fur*) and BW25113 $\Delta mntR::kan$ (lacking *mntR*) were obtained from the
765 Keio collection (strains JW0669 and JW0801, respectively). The kanamycin resistance cassette from
766 BW25113 $\Delta mntR::kan$ was removed using helper plasmid pCP20 carrying FLP recombinase and
767 $\Delta fur::kan$ fragment was moved into strain BW25113 $\Delta mntR$ (*kan* cassette removed) by P1
768 transduction. The remaining kanamycin resistance cassette was removed and genotype ($\Delta mntR/\Delta fur$)
769 confirmed by PCR using primers 35-38 (Supplementary Table 5). *E. coli* BW25113 strains were
770 cultured to logarithmic phase in M9 minimal medium supplemented with thiamine (10 $\mu\text{g ml}^{-1}$), and 1
771 μM ferric citrate (BW25113 $\Delta zntR/\Delta zur$ and BW25113 $\Delta nikR/\Delta rcnR$) or 100 μM FeSO_4
772 (BW25113 $\Delta mntR/\Delta fur$). *Salmonella* SL1344 was grown as described for transcript abundance
773 determination of *iroB*. Purified stocks of MntR, Fur, RcnR, NikR, CueR, Zur, and ZntR were
774 quantified by amino acid analysis (UC Davis). Purification of recombinant RcnR, Zur and ZntR, and
775 their quantitation in *Salmonella* cells cultured with ZnSO_4 (ZntR and Zur), or CoCl_2 (RcnR) was
776 performed as described for quantitation in cells cultured without metal supplementation¹¹.
777 Quantitation of MntR, Fur, NikR and CueR (in cells with and without cognate metal supplementation)
778 was performed as for Zur and ZntR¹¹. Standard curve samples were prepared by dilution of purified
779 protein stocks into cell lysates from BW25113 $\Delta mntR/\Delta fur$ (MntR and Fur), SL1344 $\Delta cueR/\Delta golS$
780 (CueR). Heavy isotope labelled peptides ($[^{13}\text{C}_6, ^{15}\text{N}_4]$ arginine residues; Thermo Fisher) were used as
781 working internal standards (IS). Samples were prepared and analysed by scheduled multiple reaction
782 monitoring (MRM) mass spectrometry, as previously described¹¹. A quadratic $1/x^2$ weighted
783 regression model was used to perform standard curve calibration (Supplementary Fig. 8a). The
784 transitions monitored were: 765.4/746.2 for Zur peptide ETEPQAKPPTIYR (770.4/756.2 for IS),

785 550.8/601.3 for ZntR peptide LADVTPDITR (555.8/611.3 for IS), 409.2/590.3 for RcnR peptide
 786 GAVNGLMR (414.2/600.3 for IS), 500.3/730.4 for MntR peptide LGVSQPTVAK (504.3/738.4 for
 787 IS), 426.8/482.3 for CueR peptide GLVTPPLR (431.8/492.3 for IS), 690.8/1039.5 for Fur peptide
 788 VIEFSDDSIEAR (695.8/1049.5 for IS), 937.4/1171.6 for NikR peptide GDMGDVQHFADDVIAQR
 789 (942.4/1181.6 for IS).

790

791 **Mathematical calculations.** Fractional occupancy of DNA targets with sensor (θ_D or θ_{DM} ; Fig. 1b), as
 792 a function of metal concentration ($[M]$), was calculated using metal affinities (K_1), DNA affinities (K_3
 793 and K_4), cellular abundance of each sensor (P_T), and number of DNA target(s) (D) (Table 1 and
 794 Supplementary Figs. 8b, Supplementary Table 8). P_T was calculated using determined sensor
 795 concentrations in *Salmonella* cells grown without (P_0) and with supplementation of cognate metal (P_1)
 796 (Supplementary Fig. 8b), by relating fractional change in DNA occupancy to fractional change in
 797 protein abundance (Equations 2 and 3):

$$798 \quad \frac{P_T - P_0}{P_1 - P_0} = \frac{\theta_D - \theta_{D0}}{\theta_{D1} - \theta_{D0}} \quad (2)$$

799

$$800 \quad \frac{P_T - P_0}{P_1 - P_0} = \frac{\theta_{DM} - \theta_{DM0}}{\theta_{DM1} - \theta_{DM0}} \quad (3)$$

801 Where θ_{D0} and θ_{D1} are DNA occupancies with sensor (θ_{DM0} and θ_{DM1} for metalated sensor) at low and
 802 high cognate metal concentrations, respectively. A cell volume of 1 fl was used to calculate cellular
 803 concentrations of P_0 , P_1 and D_T from values in Table 1 and Supplementary Figs. 8b and
 804 Supplementary Table 1. Equations expressing θ_D and θ_{DM} as a function of $[M]$, were derived
 805 (Supplementary Note 2), and a template Excel spreadsheet enables calculation of θ_D or θ_{DM}
 806 (Supplementary Dataset). DNA occupancy of each sensor was normalised for inter-comparison using
 807 the minimum and maximum DNA occupancy values.

808 Fractional DNA occupancy inferred from K_1 only, to generate Supplementary Fig. 10a, was
 809 calculated using Equation 4:

$$810 \quad \theta_S = \frac{[M]K_1}{(1 + [M]K_1)} \quad (4)$$

811 Where θ_S is the fractional occupancy of sensor with metal.

812 Simulations in Supplementary Figs. 10, 12 and 14 were generated by changing one or more
813 parameter(s) as specified in the figure legend.

814 DNA binding affinities at 500 mM salt were calculated based on apo-Zur, Zn(II)-Zur and apo-
815 NikR data, then used to determine DNA occupancies, as described in Supplementary Note 2.

816 Non-specific DNA affinities for MntR, Fur, RcnR, NikR, ZntR and CueR were estimated
817 based on determined Zur affinities for *nixA*Pro as described in Supplementary Note 2. To incorporate
818 competition from non-specific DNA, further equations were derived (Supplementary Note 2) to
819 calculate θ_D or θ_{DM} . In this case a supplementary dataset (spreadsheet) is not provided due to the
820 complexity of the calculation. DNA occupancy of each sensor was normalised for inter-comparison
821 using the minimum and maximum DNA occupancy values (Supplementary Fig. 13).

822 The buffered [M] corresponding to a normalised fractional DNA occupancy (θ_D or θ_{DM}) of 0.5
823 was determined for each sensor and indicates the available [M] in the *Salmonella* cytosol (MATLAB
824 codes in Supplementary Note 3). The binding affinity (K_A) of a metalloprotein required for 20, 50 and
825 80% metal occupancy at these buffered [M] was calculated using Equation 5:

$$826 \quad K_A = \frac{\theta_P}{[M](1 - \theta_P)} \quad (5)$$

827 K_A was used to calculate the standard free-energy for formation (ΔG°) of the protein-metal complex
828 using Equation 6 to generate Fig. 4c:

$$829 \quad \Delta G^\circ = -RT \ln K_A \quad (6)$$

830 Where $R = 8.314 \times 10^{-3}$ KJ mol⁻¹K⁻¹ and $T = 298.15$ K.

831 The concentration of Zn(II) ions associated with the buffer (Fig. 4b), was calculated using
832 Equation 7:

$$833 \quad [M_T] = \frac{K_5[M]^2 + [M](K_5[B_T] + 1)}{(1 + K_5[M])} \quad (7)$$

834 Where K_5 is the buffer Zn(II)-affinity and $[B_T]$ is the concentration of buffering species
835 (Supplementary Note 2). [Zn(II)] was converted to ions cell⁻¹ using a cell volume of 1 fl.

836

837 **Metal content of *Salmonella* cells.** *Salmonella* SL1344 was grown as described for transcript
838 abundance determination of *iroB*, and an aliquot used for cell enumeration on LB agar. Cell pellets
839 (from 100 ml cultures) were washed once with 0.5 M sorbitol, 100 μ M EDTA, 10 mM HEPES pH
840 7.8, and twice in the same buffer without EDTA (all 10 ml). Pellets were suspended in ultrapure 65%
841 (v/v) HNO₃ (1 ml) to digest before metal analysis by ICP-MS.

842

843 **Metalation of sirohydrochlorin.** BL21*(DE3)plysS transformed with pETcoco-2ABCDC was
844 cultured and overexpression induced as described previously (overnight expression at 20 °C)³⁹. Cell
845 pellets suspended in 100 mM NaCl, 10 mM imidazole, 20 mM Tris pH 8.0 for lysis. Following lysis
846 and clarification, lysate was applied to 5 ml HisTrap HP (GE Healthcare) equilibrated with suspension
847 buffer. Column was washed with suspension buffer (10 CV), then suspension buffer containing 60
848 mM imidazole (5 CV), before elution with suspension buffer containing 400 mM imidazole. In an
849 anaerobic glovebox the peak (2.5 ml) elution fraction was applied to a Sephadex G25 equilibrated in
850 anaerobic 100 mM NaCl, 50 mM Tris pH 8.0 and eluted directly into solution A using the same
851 buffer. Solution A contained 20 mg *S*-adenosyl-L-methionine, 10 mg aminolevulinic acid and 6.5 mg
852 nicotinamide adenine dinucleotide dissolved in 2 ml anaerobic 100 mM NaCl, 50 mM Tris pH 8.0 and
853 adjusted to pH 8.0 with NaOH. Light excluded and left overnight. Reaction product applied to 1 ml
854 HiTrap DEAE FF (GE Healthcare) equilibrated in anaerobic 100 mM NaCl, 20 mM Tris pH 8.0.
855 Column washed with equilibration buffer containing 100, 200, 300 mM NaCl (10 CV each) and
856 eluted with equilibration buffer containing 800 mM NaCl. Sirohydrochlorin quantified via $\epsilon_{376\text{ nm}} =$
857 240,000 M⁻¹ cm⁻¹.

858 Co(II) insertion into sirohydrochlorin was performed in anaerobic 100 mM NaCl, 400 mM
859 KCl, 10 mM HEPES pH 7.0 (absence of metal buffer) or 50 mM HEPES pH 7.0 (presence of metal
860 buffer). Supplementary Equations 34-38 (Supplementary Note 2) were used to define buffered
861 [Co(II)], at a certain [NTA] and [Co(II)], with the NTA Co(II) association constant at pH 7.0 ($4.5 \times$
862 10^7 M⁻¹) determined using Schwarzenbach's α co-efficient. 2.8 mM NTA will buffer 300 μ M Co(II)
863 at 2.7×10^{-9} M, approximating the calculated intracellular buffered [Co(II)] (2.5×10^{-9} M). For Co(II)
864 insertion in the absence of metal buffer 50 μ M CoCl₂ was added to a solution of ~ 5 μ M

865 sirohydrochlorin in the absence or presence of 5 μM CbiK. For Co(II) insertion in the presence of
866 metal buffer ~ 5 μM sirohydrochlorin with or without 5 μM CbiK was added to a solution of 2.8 mM
867 NTA and 300 μM Co(II). Decrease in $A_{376\text{ nm}}$ was monitored ($\lambda 35$ UV-visible spectrophotometer).
868 Under each condition reactions with enzyme run to equilibrium were used to define an extinction
869 coefficient for Co(II)-loaded sirohydrochlorin.

870 CbiK metal occupancy in the cell was calculated using Equation 8:

$$871 \quad \theta = \frac{[M]_{buffered}}{K_D + [M]_{buffered}} \quad (8)$$

872 Where θ is fractional protein occupancy with metal, K_D is CbiK metal dissociation constant and
873 $[M]_{buffered}$ is the calculated intracellular buffered metal concentration.

874

875 **Statistics and reproducibility**

876 Sample sizes followed convention in the literature for equivalent analyses. To enable calculation of
877 s.d. in experiments designed to derive quantitative values to be used in the simulations these assays
878 were initially performed in triplicate or quadruplicate (where equipment allowed even numbers of
879 samples) with additional replicates performed when the s.d. was initially high. The number of
880 independent experiments or biologically independent samples is shown for each result.

881

882 **Data availability**

883 All source data are available within the article and its Supplementary Information files, or from the
884 corresponding author upon request. Correspondence and requests for materials should be addressed to
885 nigel.robinson@durham.ac.uk.

886

887 **Code availability**

888 Equation derivations, template Excel spreadsheet (with instructions) and MATLAB codes (with
889 instructions) are available in Supplementary Note 2, Supplementary Dataset and Supplementary Note
890 3, respectively.

891 **Methods-only References**

892 51 Chivers, P. T., Benanti, E. L., Heil-Chapdelaine, V., Iwig, J. S. & Rowe, J. L. Identification of
893 Ni-(L-His)₂ as a substrate for NikABCDE-dependent nickel uptake in *Escherichia coli*.
894 *Metallomics* **4**, 1043-1050 (2012).

895 52 Livak, K. J. & Schmittgen, T. D. Analysis of relative gene expression data using real-time
896 quantitative PCR and the 2^{-ΔΔCT} method. *Methods* **25**, 402-408 (2001).

897 53 Ramakers, C., Ruijter, J. M., Deprez, R. H. L. & Moorman, A. F. M. Assumption-free
898 analysis of quantitative real-time polymerase chain reaction (PCR) data. *Neurosci. Lett.* **339**,
899 62-66 (2003).

900 54 Chivers, P. T. & Sauer, R. T. NikR repressor: high-affinity nickel binding to the C-terminal
901 domain regulates binding to operator DNA. *Chem. Biol.* **9**, 1141-1148 (2002).

902 55 Romao, C. V. *et al.* Evolution in a family of chelatascs facilitated by the introduction of
903 active site asymmetry and protein oligomerization. *Proc. Natl. Acad. Sci. U S A* **108**, 97-102
904 (2011).

905 56 Stookey, L. L. Ferrozine-a new spectrophotometric reagent for iron. *Anal. Chem.* **42**, 779-781
906 (1970).

907 57 Dainty, S. J., Patterson, C. J., Waldron, K. J. & Robinson, N. J. Interaction between
908 cyanobacterial copper chaperone Atx1 and zinc homeostasis. *J. Biol. Inorg. Chem.* **15**, 77
909 (2010).

910 58 Kuzmic, P. Program DYNAFIT for the analysis of enzyme kinetic data: application to HIV
911 proteinase. *Anal. Biochem.* **237**, 260-273 (1996).

912 59 Reyes-Caballero, H., Lee, C. W. & Giedroc, D. P. *Mycobacterium tuberculosis* NmtR harbors
913 a nickel sensing site with parallels to *Escherichia coli* RcnR. *Biochemistry* **50**, 7941-7952
914 (2011).

915 60 Xiao, Z. *et al.* Unification of the copper(I) binding affinities of the metallo-chaperones Atx1,
916 Atox1, and related proteins: detection probes and affinity standards. *J. Biol. Chem.* **286**,
917 11047-11055 (2011).

918
919

920
 921
 922
 923
 924
 925
 926
 927
 928
 929
 930
 931
 932
 933
 934
 935
 936
 937

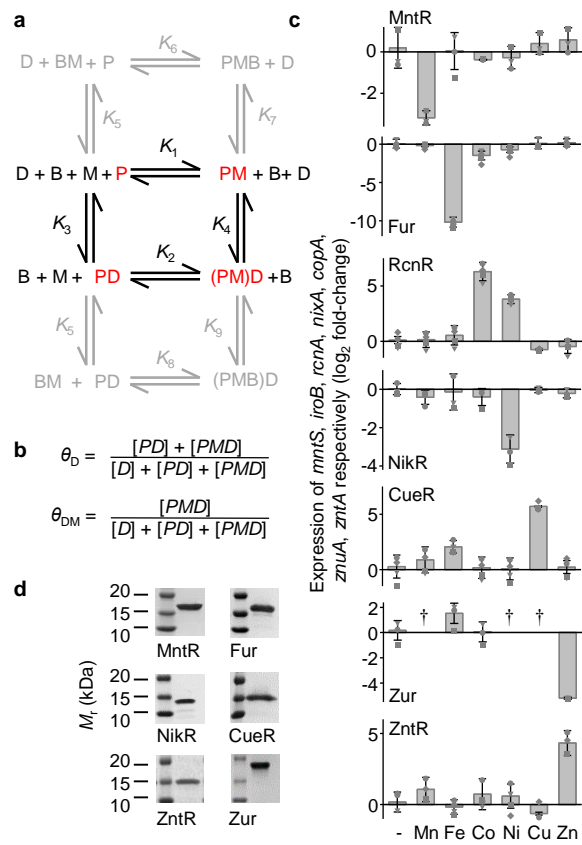


Figure 1 | Metal binding and DNA binding are coupled to enable *Salmonella* to sense different metals.

938
 939
 940
 941
 942
 943
 944
 945
 946
 947
 948
 949
 950
 951
 952
 953
 954
 955

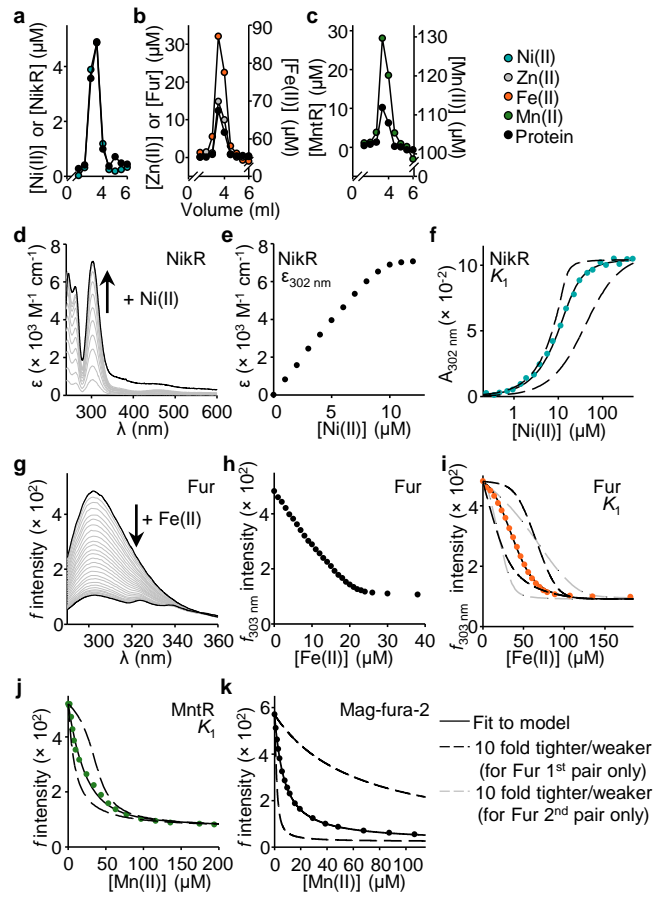


Figure 2 | Metal affinities that complete a set of values for *Salmonella* metal sensors.

956

957

958

959

960

961

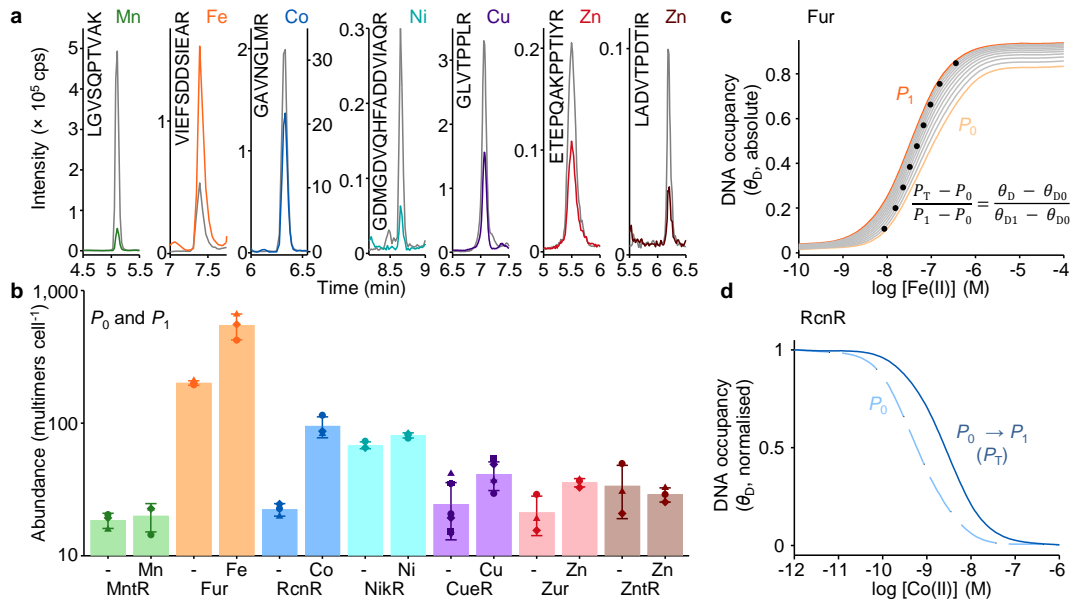
962

963

964

965

966



967 **Figure 3 | Metals change the abundance of some sensors to modify regulation.**

968

969
 970
 971
 972
 973
 974
 975
 976
 977
 978
 979
 980
 981
 982
 983
 984
 985
 986
 987
 988

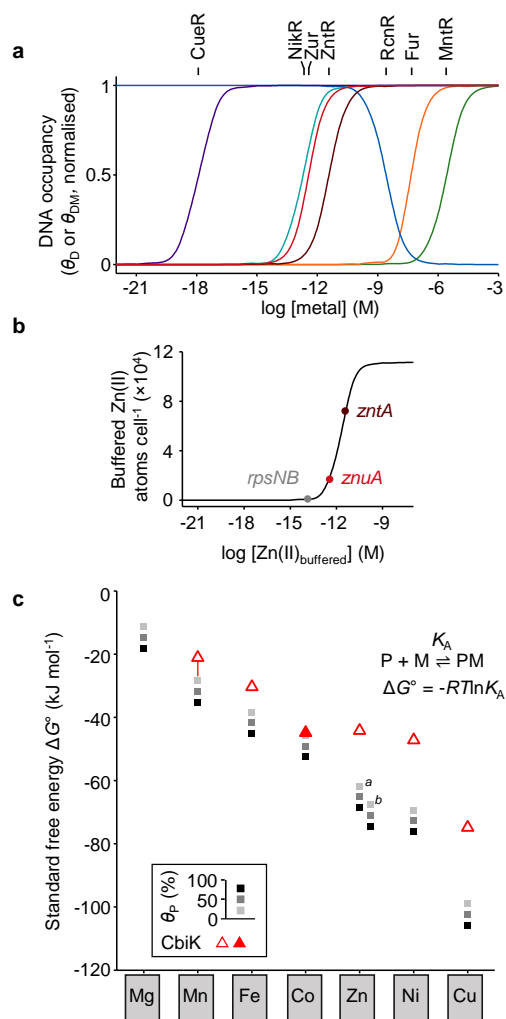


Figure 4 | Sensing is tuned to the Irving-Williams series.

989
 990
 991
 992
 993
 994
 995
 996
 997
 998
 999
 1000
 1001
 1002
 1003
 1004
 1005

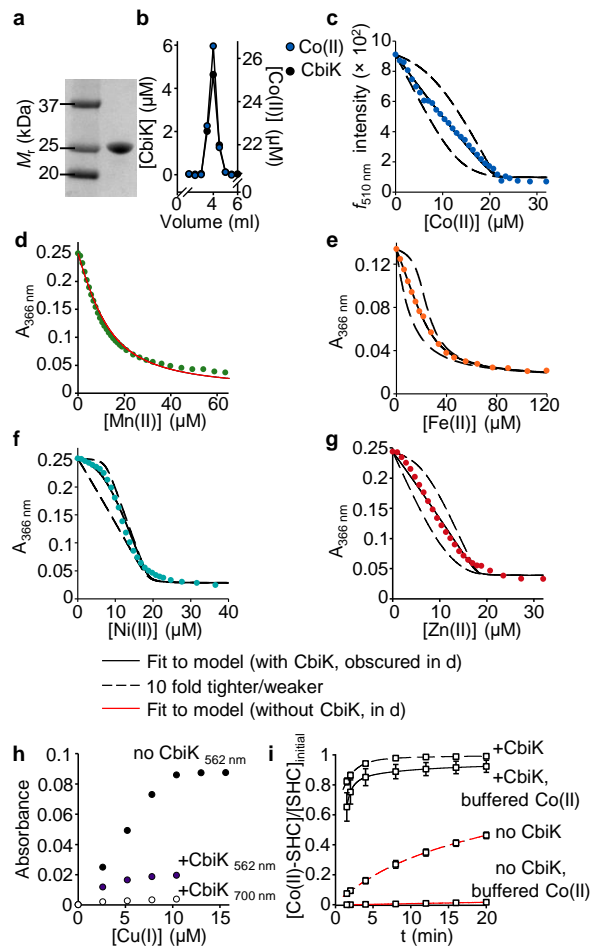


Figure 5 | Metalation of CbiK and sirohdrochlorin.